The Validity of the Reynolds Equation in Modeling Hydrostatic Effects in Gas Lubricated Textured Parallel Surfaces

Y. Feldman

Y. Kligerman[1]
Mem. ASME
e-mail: mermdyk@tx.technion.ac.il

I. Etsion
Fellow ASME

S. Haber
Mem. ASME

Department of Mechanical Engineering,
Technion-Israel Institute of Technology,
Faculty of Mechanical Engineering,
Technion City, Haifa, 32000, Israel

Microdimples generated by laser surface texturing (LST) can be used to enhance performance in hydrostatic gas-lubricated tribological components with parallel surfaces. The pressure distribution and load carrying capacity for a single three-dimensional dimple, representing the LST, were obtained via two different methods of analysis: a numerical solution of the exact full Navier-Stokes equations, and an approximate solution of the much simpler Reynolds equation. Comparison between the two solution methods illustrates that, despite potential large differences in local pressures, the differences in load carrying capacity, for realistic geometrical and physical parameters, are small. Even at large clearances of 5% of the dimple diameter and pressure ratios of 2.5 the error in the load carrying capacity is only about 15%. Thus, for a wide range of practical clearances and pressures, the simpler, approximate Reynolds equation can safely be applied to yield reasonable predictions for the load carrying capacity of dimpled surfaces.
[DOI: 10.1115/1.2148419]

1 Introduction

Surface texturing in general and laser surface texturing (LST) in particular has gained an increasing interest in recent years as a means for enhancing tribological performance [1]. Several theoretical models based on solving the Reynolds equation, e.g., [2–5] were developed so far for LST tribological components. Although these models showed good agreement with experimental results (see [3–5]) it was argued on several occasions that the Reynolds equation may not be valid for the particular LST parameters in use and that the full Navier-Stokes (NS) equations should be employed. The LST produces on one of the mating surfaces a large number of microdimples having typically a depth over diameter ratio of order $10^{-2} - 10^{-1}$, pitch over diameter ratio of order 10^0, and depth over clearance ratio that can reach an order of 10^1. Thus, a discussion of the validity limits of the lubrication theory and the Reynolds equation for solving LST problems seems appropriate.

A detailed analysis of the lubrication theory validity, its limitations, and the effect of fluid inertia was performed in 1985 by Tichy and Chen [6] for the case of an infinitely long slider bearing with completely smooth inclined surfaces. Experimental results showed that the theory predicts the correct trends and that fluid inertia can double the load capacity at modified Reynolds number (Re of about 10) compared to that predicted by the Reynolds equation. In the range of modified Re number below unity the fluid inertia effect was found negligible and the difference between the NS equations solution and the hydrodynamic lubrication theory was insignificant.

Several analyses were published in recent years that evaluated the validity of the Reynolds equation in cases where surface roughness is included. This was done by comparing pressure distributions and load capacities obtained from the Stokes or NS equations with these obtained from the Reynolds equation. Arghir

et al. [7] treated the case of laminar, isothermal, shear driven flow between closely spaced parallel walls of which one has a regular macro-roughness pattern of rectangular, sinusoidal, or triangular grooves. The wavelength and amplitude of each pattern was of the same order as the distance between the walls. It was shown that with increasing magnitude of the convective inertia, all macro-roughness patterns produced a net lift force. Such a load cannot be obtained from the Reynolds equation in symmetric converging diverging film thickness geometries if cavitation is not considered and the pressure distribution is antisymmetric. In [7] the possibility of cavitation in low pressure regions was completely overlooked by the authors thus making their comparison questionable.

Odyck and Venner [8] investigated the validity of the Reynolds equation for iso-viscous, Newtonian and incompressible flow between two surfaces having roughness in the form of a sinus wave. Both the Stokes and the Reynolds equations were solved to obtain and compare the pressure distributions and load carrying capacities. It was found that the differences between the two solutions depend on the ratio of the film thickness to the roughness feature wavelength. Cavitation was considered by simply eliminating negative pressures (half Sommerfeld cavitation condition).

Song et al. [9] used the full NS equations to find the validity limits of the Reynolds equation in the case of an incompressible lubricating flow between a fixed upper sinusoidal wall with one period and a lower plate moving with a constant speed. Results were obtained for an extremely low Reynolds number in the order of 10^{-6}. The differences in the maximum pressure obtained from the NS and lubrication theory where very small when the average film thickness was 0.075 μm but became large when this thickness was five times larger.

Sahlin et al. [10] studied the effect of two-dimensional (2D) micro-patterned surfaces in hydrodynamic lubrication between two parallel walls. The pressure distribution and the load carrying capacity obtained from the Stokes and the NS equations were compared for different Reynolds numbers and pattern geometry parameters. The authors concluded that the micropattern on one of the surfaces causes an appreciable load carrying capacity mainly due to the advective terms in the NS equations. However, the

---
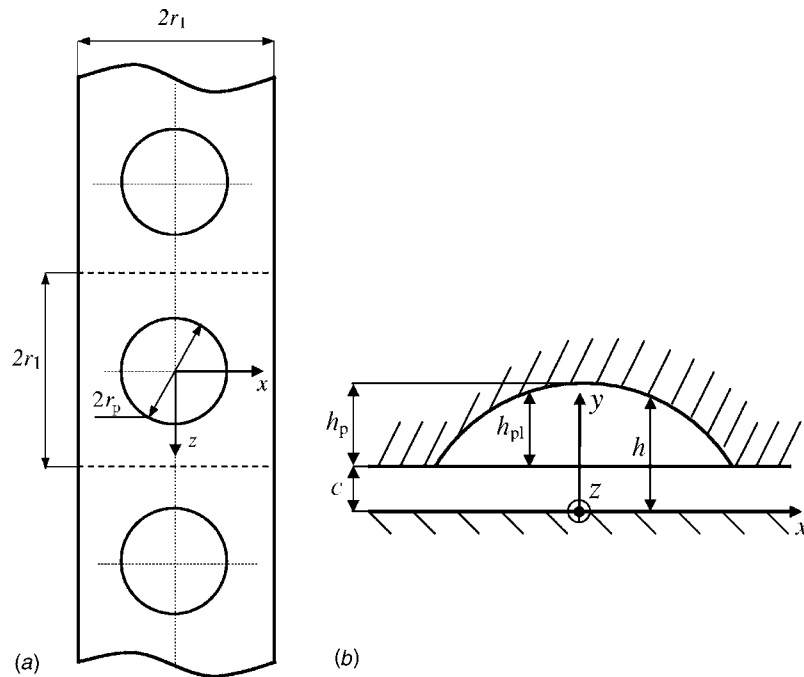
Fig. 1   The geometrical model: (*a*) a segment of infinitely long strip of dimples; (*b*) a cross section at the middle of one imaginary cell

authors completely overlooked potential effect of cavitation on their pressure distribution. This neglected effect could well contribute to load capacity even without considering the advective terms.

In Refs. [7–10] the authors either neglected completely or treated potential cavitation effect on load capacity with a simplistic approach (either Sommerfeld or half Sommerfeld conditions) and hence, their conclusions regarding the validity of the Reynolds equation for incompressible lubricants may be inaccurate. When dealing with compressible lubricants the cavitation is not an issue and, hence, a clearer picture of the validity of the lubrication theory for textured surfaces can be obtained.

Guardino et al. [11] studied both incompressible and compressible flows in air riding seals using computational fluid dynamics (CFD) analysis for the NS equations, and analytical/numerical solutions for the Reynolds equation. The authors treated various two-dimensional roughnesses in the form of sinusoidal waves on an infinite Rayleigh step geometry of the stationary wall. It was observed that surface roughness can have dramatic effects on the streamline patterns, and can result in extensive recirculation regions, particularly for large values of roughness amplitude to clearance ratio. One of the main conclusions of the study is that the CFD and Reynolds solutions are in good agreement for low values of the roughness amplitude to clearance ratio. At higher values of roughness amplitude to clearance ratio the Reynolds equation solution underestimates the load carrying capacity compared to the CFD results. The differences found between the Reynolds equation and CFD solutions were larger in the case of incompressible flow compared to the case of compressible one.

Compressible Stokes flow in thin films was investigated by Odyck and Venner [12]. The authors studied the differences between load capacities obtained from solutions of the Reynolds and Stokes equations for laminar flow of a compressible medium in a thin film containing rectangular slot geometry. They found that in spite of local differences in the pressure at the edges of the rectangular slot, the two different solutions for the load carrying capacity are in good agreement.

Almqvist and Larsson [13] investigated the validity of the Reynolds equation for lubricant film flows in the presence of a 2D ridge surface roughness located on the stationary surface. Newtonian, non-Newtonian, piezoviscous and compressible fluids were considered. It was found that when the ratio of film thickness to wave length is of order 10^{-2} or less the Reynolds equation is a good approximation with less than 3% error in the maximum pressure and in the pressure difference across the fluid film. When the above ratio is of order 10^{-1} the deviations between the Reynolds and the full CFD solutions become up to 8% in the maximum pressure and up to 30% in the pressure difference across the fluid film.

The comparisons made by Almqvist and Larsson [13] addressed the local pressure extremum vis-á-vis the load carrying capacity. They showed that although the error in the pressure field may be large, the integrated effect in the form of load carrying capacity may be small and even negligible.

From the foregoing literature survey it seems that no clear conclusion yet exists regarding the validity limits of the Reynolds lubrication theory for cases of surface texture like LST. It is the purpose of the present work to clarify this issue for the case of a hydrostatic compressible gas flow, applicable, for example, in high pressure LST gas seals. This will be accomplished by comparing the pressure distribution and the load carrying capacity obtained from a CFD solution of the NS equations and these obtained from the Reynolds equation.

2   Analytical Model

Figure 1(*a*) shows a segment of an infinitely long stationary strip of microdimples. The dimples have a spherical geometry with a base radius r_p. Each dimple is located within an imaginary rectangular cell of sides $2r_1 \times 2r_1$. A cross section through one of the dimples is presented in Fig. 1(*b*) showing the dimple depth h_p and its location on a top surface that is separated by a nominal clearance, c, from another bottom stationary flat and smooth surface. The origin of a coordinate system (x,y,z) is located at the bottom surface just below the center of the dimple as shown in Fig. 1(*b*). The x axis points in the direction of a pressure drop. The local film thickness h between the nominally parallel surfaces is given by

$$h = \begin{cases} c + h_{pl}(x,z) & \sqrt{x^2 + z^2} \leqslant r_p \\ c & \sqrt{x^2 + z^2} > r_p \end{cases} \tag{1}$$

where the local dimple depth h_{pl} is:

$$h_{pl}(x,z) = \sqrt{\left(\frac{h_p^2 + r_p^2}{2h_p}\right)^2 - (x^2 + z^2)} - \frac{r_p^2 - h_p^2}{2h_p} \tag{2}$$

The full three-dimensional Navier-Stokes equations for steady state Newtonian ideal gas in a laminar flow, neglecting external forces, are:

$$\rho u_i \frac{\partial u_j}{\partial x_i} = -\frac{\partial p}{\partial x_j} - \frac{\partial}{\partial x_j}\left(\frac{2}{3}\mu \frac{\partial u_i}{\partial x_i}\right) + \frac{\partial}{\partial x_i}\left[\mu\left(\frac{\partial u_i}{\partial x_j} + \frac{\partial u_j}{\partial x_i}\right)\right] \tag{3}$$

where i and j are dummy and free indices, respectively.

The steady state continuity equation for compressible gas flow is:

$$\frac{\partial}{\partial x_i}(\rho u_i) = 0 \tag{4}$$

Note that the coordinates x_1, x_2, and x_3 in Eqs. (3) and (4) stand for x, y, and z, respectively.

Assuming an isothermal flow, the ideal gas state equation is given by:

$$\frac{p}{\rho} = \text{const} \tag{5}$$

Equations (3)–(5) represent the steady state five scalar equations for the five unknown functions: the three velocity components, the pressure, and the density fields. The appropriate no slip boundary conditions for the velocity at the two stationary walls (see Fig. 1(b)) are:

$$\mathbf{u}(x,y=0,z) = \mathbf{u}(x,y=h,z) = 0 \tag{6}$$

The inlet and outlet pressure boundary conditions are:

$$p(x=-r_1,y,z) = p_o; \quad p(x=r_1,y,z) = p_a \tag{7}$$

Periodicity of the surface texturing in the z direction, and symmetry (see Fig. 1(a)) about the x axis, permit solving the pressure and velocity distributions within just one half of one imaginary cell. From the periodicity, symmetry, and continuity of the velocity distribution it follows that:

$$u_z(x,y,z=r_1) = u_z(x,y,z=0) = 0 \tag{8}$$

The 2D, steady state form of the Reynolds equation for a compressible, Newtonian, hydrostatic, ideal gas flow is given by:

$$\frac{\partial}{\partial x}\left(ph^3 \frac{\partial p}{\partial x}\right) + \frac{\partial}{\partial z}\left(ph^3 \frac{\partial p}{\partial z}\right) = 0 \tag{9}$$

with the appropriate boundary conditions:

$$p(x=-r_1,z) = p_o; \quad p(x=r_1,z) = p_a \tag{10}$$

$$\frac{\partial p}{\partial z}(x,z=-r_1) = \frac{\partial p}{\partial z}(x,z=0) = 0 \tag{11}$$

3 Numerical Solution

Equation (9) is rendered dimensionless by using r_p and c to scale lengths and p_a to scale the pressure field, namely

$$X = \frac{x}{r_p}; \quad Z = \frac{z}{r_p}; \quad P = \frac{p}{p_a}; \quad H = \frac{h}{c}; \tag{12}$$

The dimensionless local film thickness, $H(X,Z)$, is given by:

$$H(X,Z) = \begin{cases} 1 + \sqrt{\left(\frac{\varepsilon}{2\delta} + \frac{1}{8\varepsilon\delta}\right)^2 - \frac{1}{4\delta^2}(X^2 + Z^2)} - \left(\frac{1}{8\varepsilon\delta} - \frac{\varepsilon}{2\delta}\right) & X^2 + Z^2 < 1 \\ 1 & X^2 + Z^2 \geqslant 1 \end{cases} \tag{13}$$

where $\varepsilon = h_p/2r_p$ is the dimple aspect ratio, and $\delta = c/2r_p$ is the dimensionless clearance. Substitution of the dimensionless parameters into Eq. (9) yields the Reynolds equation in its dimensionless form:

$$\frac{\partial}{\partial X}\left(PH^3 \frac{\partial P}{\partial X}\right) + \frac{\partial}{\partial Z}\left(PH^3 \frac{\partial P}{\partial Z}\right) = 0 \tag{14}$$

Equation (14) is nonlinear, but by introducing a new dimensionless variable Q defined as:

$$Q = P^2 \tag{15}$$

it may be rewritten as a linear partial differential equation for Q:

$$\frac{\partial}{\partial X}\left(H^3 \frac{\partial Q}{\partial X}\right) + \frac{\partial}{\partial Z}\left(H^3 \frac{\partial Q}{\partial Z}\right) = 0 \tag{16}$$

Equation (16) can be solved for the Q distribution over a range of the dimensionless parameters δ and ε (see Eq. (13)), and the relevant boundary conditions (10) and (11) for Q:

$$Q(x=-R_1,Z) = P_o^2, \quad Q(X=R_1,Z) = 1 \tag{17}$$

$$\frac{\partial Q}{\partial Z}(X,Z=R_1) = \frac{\partial Q}{\partial Z}(X,Z=0) = 0 \tag{18}$$

where $R_1 = r_1/r_p$.

A finite difference method using a non-uniform grid was used to solve the Reynolds Eq. (16) with boundary conditions (17) and (18). The discretization of Eq. (16) leads to a set of linear algebraic equations for the nodal values of $Q(X,Z)$. This equation set was solved using a successive over-relaxation Gauss–Seidel iterative method. The solution of Eq. (16) provides, through the transformation (15), a pressure distribution that can be integrated over the cell area to obtain its load carrying capacity.

The full NS equations were solved using a commercial finite element software ANSYS/FLOTRAN. A tetrahedral element "FLUID 142" was used with a denser grid within the dimple and near its boundary where the film thickness gradient is discontinuous. Additional refinement of elements was done near the stationary top and bottom walls where significant velocity gradients can exist. The tri-diagonal matrix algorithm (TDMA) and preconditioned conjugate residual solvers were used to obtain the velocity and pressure distributions, respectively.

The comparison between the solutions of the Reynolds equation and the full NS equations was performed for a typical LST case of a dimple having a diameter $2r_p = 100~\mu$m. The range of dimple depth was $5~\mu$m $\leqslant h_p \leqslant 50~\mu$m and of the clearance $1~\mu$m $\leqslant c \leqslant 5~\mu$m. These values correspond to a range of the dimensionless parameters ε from 0.05 to 0.5 and δ from 0.01 to 0.05, respectively. The value of $h_p = 5~\mu$m characterizes a shallow dimple while the value of $h_p = 50~\mu$m is the maximum possible depth of a hemispherical dimple.
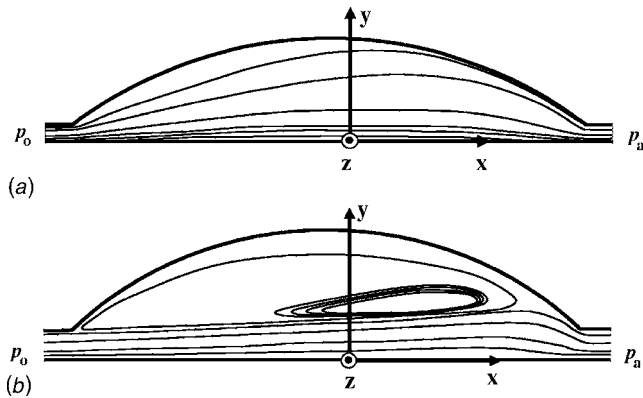
Fig. 2 Streamlines of the gas flow at the mid cross section of a dimple: (*a*) without flow recirculation, *c*=3 μm, h$_p$=15 μm; (*b*) with flow recirculation at the top of the dimple, *c*=5 μm, h$_p$=20 μm

Fig. 3 Transition from recirculation (above) and no circulation (below) and the recirculation inception line as function of the aspect ratio ε and dimensionless clearance δ
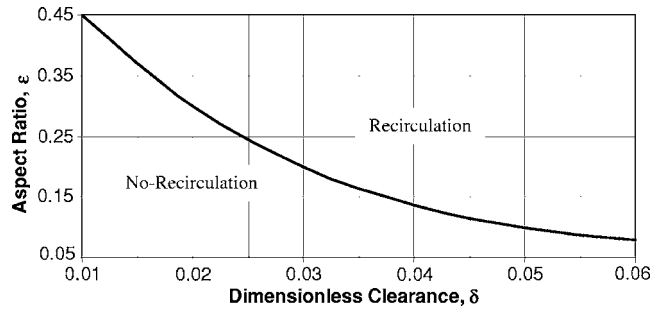
A length $2r_1=110$ μm was selected for the imaginary cell. This results in very large area density of the dimples where each dimple covers 65% of its cell area leaving only 5 μm between the cell and dimple boundaries. The very large area density was selected to represent an extreme case where the largest deviations between the Reynolds and the NS solutions may be expected. The dynamic viscosity μ was 18.21×10^{-6} Pa s (air dynamic viscosity at 20°C), and the pressure drop across the dimples strip was 0.1 MPa, which is a typical value for, for example, hydrostatic gas seals.

The non-uniform grid for solving the Reynolds equation had 33 divisions along the dimple radius and additional 22 divisions outside the dimple. Convergence and accuracy were acceptable when the difference in the pressure distribution between two consecutive iterations was less than 1%. Convergence and accuracy of the finite element solution of the NS equations was ensured by doubling the number of elements until the difference in load carrying capacity was less that 1%. This resulted in 80,000–110,000 nodes depending on the dimple depth.

4 Results and Discussion

4.1 Inception of Recirculation in the Flow Field. A basic assumption for the validity of the Reynolds equation states that compared to the velocity gradients $\partial u_x / \partial y$ and $\partial u_z / \partial y$ all other velocity gradients are small and may be neglected. In this case a typical flow field will have homogenous streamlines with opened contours as shown in Fig. 2(*a*). On the other hand, violation of this basic assumption would lead to regions of flow recirculation with streamlines having closed contours as in Fig. 2(*b*). The inception of recirculation in the flow field was investigated for the full range of ε and δ values. The results are presented in Fig. 3 showing that for the smallest clearance $\delta=0.01$ even a very large dimple depth does not produce recirculation. As the clearance increases, recirculation inception occurs at decreasing depth.

4.2 Magnitude of Pressure Gradients Across the Film Thickness. Another assumption for the Reynolds equation validity is a negligible pressure change across the film thickness. Figures 4(*a*) and 4(*b*) present typical isobars corresponding to the cases (a) and (b) of Fig. 2, respectively. As can be seen there is a good correlation between recirculation in the flow field and appreciable pressure change across the film thickness. As shown in Fig. 4(*a*), the pressure gradients in the *y* direction are noticed only close to the dimple leading and trailing edges where a discontinuity in the film thickness gradient exists. Most of the dimple cross-section area experiences negligible pressure differences in the *y* direction. Figure 4(*b*), on the other hand, shows significant pres-

sure gradients in the *y* direction not only at the leading and trailing edges but also in the rest of the dimple cross section.
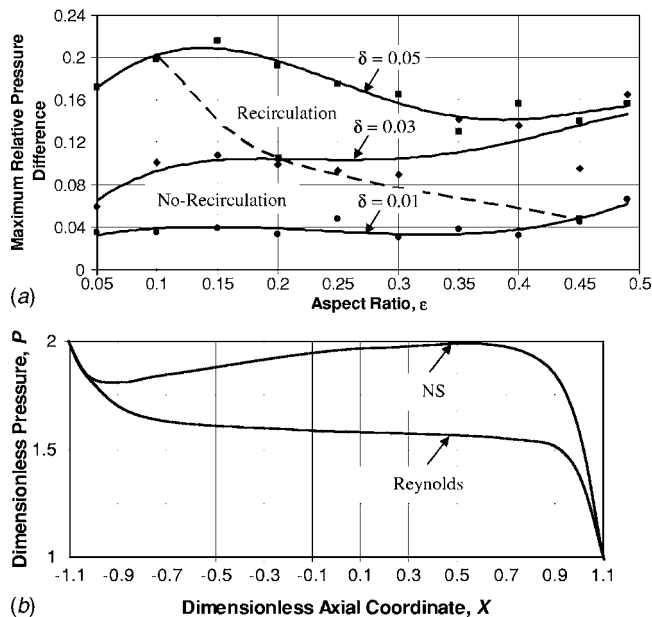
4.3 Pressure Distribution Obtained From the NS and the Reynolds Equations. Figure 5(*a*) presents the maximum relative difference between the pressure distributions that were obtained from the Reynolds equation and the NS equations. This maximum relative difference occurs at the mid cross section of the dimple. The maximum relative difference is shown versus ε for three δ values. The dashed line in Fig. 5(*a*) illustrates the locus of points related to the flow recirculation inception (see Fig. 3). As can be seen for $\delta=0.01$ and $\varepsilon \leqslant 0.4$ the maximum relative difference in the pressure distribution is less than 4%. For $\varepsilon > 0.4$ the relative difference increases and reaches about 10% at $\varepsilon=0.5$. For $\delta=0.03$ the relative difference is around 10% when $\varepsilon \leqslant 0.3$. Further increase of ε, deeper into the range of recirculation flow, leads to oscillating higher relative difference. For $\delta=0.05$ the maximum relative difference is about 22% at $\varepsilon=0.15$ (the flow recirculation inception occurs at $\varepsilon=0.1$). Further increase of ε reduces the relative difference unexpectedly to about 13% at $\varepsilon=0.35$. This unexpected behavior requires more in depth investigation which is outside the scope of the present study.

Figure 5(*b*) presents the actual dimensionless pressure distribution, along the dimple centerline, for the case of $\delta=0.05$ and $\varepsilon=0.15$. The "NS" and "Reynolds" lines are for the results obtained from the NS equations and the Reynolds equation, respectively. Clearly the pressure obtained from the NS equations is higher than that obtained from the Reynolds equation. The maximum difference of 22% occurs close to the trailing edge at about $X=0.7$. Most of the pressure change, in both cases, occurs outside the
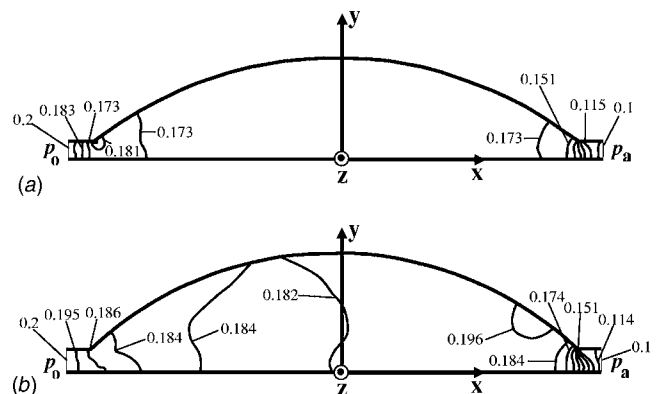

Fig. 4 Isobars (in MPa) of the gas pressure distribution at the mid cross section of a dimple obtained from the NS equations: (*a*) without flow recirculation, *c*=3 μm, h$_p$=15 μm; (*b*) with flow recirculation at the top of the dimple, *c*=5 μm, h$_p$=20 μm

(a)

(b)

Fig. 5 A comparison of the pressure distributions obtained from the NS and Reynolds equations: (a) maximum relative difference between the NS and the Reynolds equations versus dimple aspect ratio ε at various dimensionless clearance values δ; (b) the dimensionless pressure distribution at the mid cross section of the dimple for $\delta=0.05$ and $\varepsilon=0.15$

dimple boundaries (located at $X=\pm 1$) whereas inside the dimple the pressure gradient in both cases is much smaller.

4.4 Load Carrying Capacity Obtained From the NS and the Reynolds Equations. Figure 6 portrays the differences in the dimensionless load carrying capacity, W, that were obtained from the two different solutions. This parameter is obtained from the integration of the pressure over the imaginary cell area normalized by $4p_a r_1^2$. The solid lines in Fig. 6 present the results obtained from the NS equations versus the aspect ratio ε for three values of δ. The single dashed line shows the results obtained from the Reynolds equation for the entire range of ε and δ. The fact that W obtained from the Reynolds equation is independent of ε and δ was also observed in Ref. [4] for an incompressible flow. As in the case of the pressure distribution (Fig. 5(b)) the load capacity, W, obtained from the NS equations is larger than that obtained from the Reynolds equation, and the difference increases with increasing dimensionless clearance δ. The maximum difference between the results obtained from the two solutions is about 2% at $\delta=0.01$ for $\varepsilon<0.35$, 7% at $\delta=0.03$ and no more than 11% at the
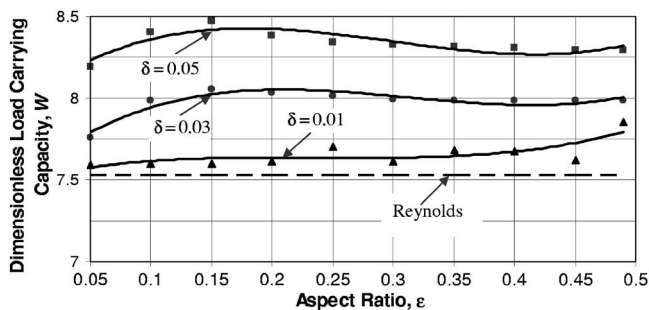
Fig. 6 Comparison of load carrying capacities, W, obtained from the NS (solid lines) and the Reynolds (dashed line) equations versus dimple aspect ratio ε at various dimensionless clearance values δ
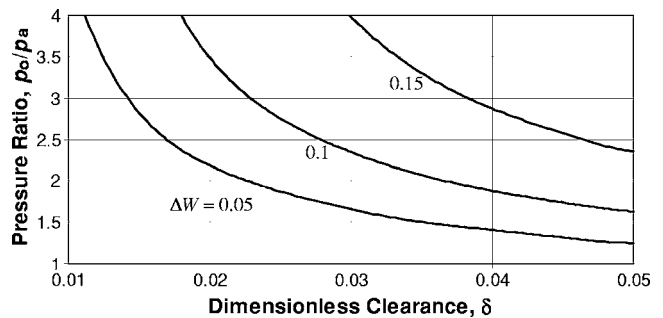
Fig. 7 A load capacity relative error map indicating that for a wide range of clearances, δ and pressure ratios, p_o/p_a, the Reynolds equation is valid.

largest clearance of $\delta=0.05$. Note that the maximum difference in load carrying capacity is about half of the relative difference in the pressure distribution for the same values of ε and δ (see Fig. 5(a)). This is due to a smoothening effect of the integrated pressure which is much less affected by large local differences in the pressure distribution. Also, the aspect ratio of the dimple, ε, has a very little effect on the load carrying capacity, W, obtained from the NS equations.

Interesting useful information was obtained when the relative error $\Delta W=1-W_{Re}/W_{NS}$ (where W_{NS} and W_{Re} are the load capacities obtained from the NS and the Reynolds equation solutions, respectively) was calculated for a wide range of the pressure ratio $1\leqslant p_o/p_a\leqslant 4$. It was found that ΔW varies linearly with p_o/p_a, is very little affected by δ (roughly as $\delta^{1/9}$) and negligibly affected by ε. Figure 7 presents an "error map" showing the combinations of p_o/p_a and δ values corresponding to a transition from a lower (under the line) to higher (above the line) value of ΔW as indicated for each of the transition boundaries. Hence, for $\delta=0.01$, for example, the Reynolds equation predicts the load capacity to within 5% of the result obtained from the NS equations throughout the full range of pressure ratios. At $\delta=0.03$ the error will be less than 5% for pressure ratio below 1.6, and more than 15% for pressure ratio above 4. These results show that for all practical values of pressures, clearances, and LST parameters the Reynolds equation is valid with respect to load capacity predictions.

5 Conclusion

A finite difference algorithm was used to solve the Reynolds equation for a hydrostatic compressible flow over a single dimple. The Reynolds equation solution was then compared with a solution of the Navier-Stokes equations for the same problem. It was found that the maximum relative difference in the pressure distribution between the above two solutions occurs in the midsection of the dimple. Significant pressure variations across the film thickness were found near the leading and trailing edges of the dimple where the film thickness gradient is discontinuous. However, these local differences have little effect on the load carrying capacity. For clearances, c, that are 3% or less of the dimple diameter the load capacity prediction by the Reynolds equation is valid over the entire range of practical dimple depth and pressure ratios. At clearances as large as 5% of the dimple diameter, and pressure ratios about 2.5, the error in the load carrying capacity may reach 15%. Thus, the use of the Reynolds equation yields reasonable load capacity predictions for a wide range of realistic clearances and pressures. For higher clearances, employment of the Reynolds equation provides a rougher estimate of the load carrying capacity. However, since in the above range of parameters the Reynolds equation underestimates the load it can safely be used.

Nomenclature

c = clearance
h_p = dimple depth

h = local film thickness inside the imaginary cell
H = dimensionless film thickness $H = h/c$
p_a = ambient pressure
p_o = high pressure
P = dimensionless pressure, $P = p/p_a$
r_p = dimple radius
u_j = velocity in j direction
$\mathbf{u}$ = velocity vector
x, y, z = Cartesian coordinates
X, Z = dimensionless coordinates, $X = x/r_p$, $Z = z/r_p$
ε = dimple aspect ratio, $\varepsilon = h_p/2r_p$
δ = dimensionless clearance, $\delta = c/2r_p$
μ = dynamic viscosity
ρ = density

References

[1] Etsion, I., 2005, "State of the Art in Laser Surface Texturing," ASME J. Tribol., **127**(1), pp. 248–253.

[2] Brizmer, V., Kligerman, Y., and Etsion, I., 2003, "A Laser Surface Textured Parallel Thrust Bearing," Tribol. Trans., **46**(3), pp. 397–403.

[3] Etsion, I., Kligerman, Y., and Halperin, G., 1999, "Analytical and Experimental Investigation of Laser-Textured Mechanical Seal Faces," Tribol. Trans., **42**(3), pp. 511–516.

[4] Etsion, I., and Halperin, G., 2002, "A Laser Surface Textured Hydrostatic Mechanical Seal," Tribol. Trans., **45**(3), pp. 430–434.

[5] Etsion, I., Halperin, G., Brizmer, V., and Kligerman, Y., 2004, "Experimental Investigation of Laser Surface Textured Parallel Thrust Bearings," Tribol. Lett., **17**(2), pp. 295–300.

[6] Tichy, J. A., and Chen, S. H., 1985, "Plain Slider Bearing Load Due to Fluid Inertia-Experiment and Theory," ASME J. Tribol., **107**(1), pp. 32–38.

[7] Arghir, M., Roucou, N., Helene, M., and Frene, J., 2003, "Theoretical Analysis of the Incompressible Laminar Flow in Macro-Roughness Cell," ASME J. Tribol., **125**(2), pp. 309–318.

[8] Odyck van, D. E. A., and Venner, C. H., 2003, "Stokes Flow in Thin Films," ASME J. Tribol., **125**(1), pp. 121–134.

[9] Song, D. J., Seo, D. K., and Shults, W. W., 2003, "A Comparison Study Between Navier-Stokes Equation and Reynolds Equation in Lubricating Flow Regime," Int. J. Kor. Soc. Mech. Eng., **17**(4), pp. 599–605.

[10] Sahlin, F., Glavatskih, S. B., Almqvist, T., and Larsson, R., 2005, "Two-Dimensional CFD-Analysis of Micro-Patterned Surfaces in Hydrodynamic Lubrication," ASME J. Tribol., **127**(1), pp. 96–102.

[11] Guardino, C., Chew, J. W., and Hills, N. J., 2004, "Calculation of Surface Roughness Effects on Air-Riding Seals," ASME J. Eng. Gas Turbines Power, **126**(1), pp. 75–82.

[12] Odyck van, D. E. A., and Venner, C. H., 2003, "Compressible Stokes Flow in Thin Films," ASME J. Tribol., **125**(3), pp. 543–551.

[13] Almqvist, T., and Larsson, R., 2004, "Some Remarks on the Validity of Reynolds Equation in the Modeling of Lubricant Film Flows on the Surface Roughness Scale," ASME J. Tribol., **126**(4), pp. 703–710.